ELSEVIER

Journal of Membrane Science 162 (1999) 199–211

journal of MEMBRANE SCIENCE

Study of series resistances in high-shear rotary ultrafiltration

Roger C. Viadero Jr.*, Ronald L. Vaughan Jr., Brian E. Reed

Department of Civil and Environmental Engineering, West Virginia University, P.O. Box 6103, Morgantown, WV 26506-6103, USA

Received 26 October 1998; received in revised form 12 April 1999; accepted 13 April 1999

Abstract

A parametric waste-specific study was conducted to determine the relationship between permeate flux, transmembrane pressure, membrane rotational speed, and feed concentration in the high-shear rotary ultrafiltration (HSRUF) of a synthetic metal working (MW) fluid. The interactions between permeate flux and operating parameters were described using the resistance-in-series (RIS) approach to flux modeling. Eighteen discrete experiments were conducted at constant MW fluid concentration/membrane rotational speed combinations at applied pressures ranging from 103 to 517 kPa (15 to 75 psig). The fouling layer resistance, R_f, was only 12% of the total membrane resistance, R'_m, and it was determined that R_f and R'_m were independent of feed concentration and membrane rotational speed. The polarization layer resistance, R_p, was the predominant rate controlling resistance in the HSRUF of the synthetic MW fluid; however, membrane rotation induced hydraulic turbulence was effective in minimizing R_p by reducing the accumulation of solute molecules on the membrane surface. An explicit form of the resistance index, Φ, was postulated based upon observations of interactions between Φ, feed MW fluid concentration, and membrane rotational speed. The RIS model was then modified with a specific form of Φ to further describe the specific interactions between flux and operating parameters. The modified model adequately predicted flux–pressure data over the range of experimental variables examined in this study. Additionally, a set-point operating pressure was determined as a function of membrane rotational speed and feed oil concentration such that the resistances R'_m and R_p were minimized.
© 1999 Elsevier Science B.V. All rights reserved.

Keywords: Ultrafiltration; Modules; Ceramic membranes; Emulsion; High-shear

1. Introduction

Metal working (MW) fluids are used in rolling mill operations to control friction between the mill and workpiece, to dissipate heat generated during the milling procedure, and to improve the surface quality of the workpiece. MW fluids are generally oil-in-water (O/W) emulsions that contain additives such as surfactants, antimicrobial agents, and antifoaming agents. After a period of time, the MW fluids must be discarded, resulting in large volumes of oily wastewaters which are often treated using conventional cross-flow ultrafiltration (UF). The UF residual has a higher oil concentration and a lower volume than the original waste stream; thus further treatment or disposal is substantially less expensive [1].

The primary limitation of conventional cross-flow UF is the large decline in permeate flux observed with

*Corresponding author. Tel.: +1-304-293-3031; fax: +1-304-293-7109; e-mail: viadero@cemr.wvu.edu

0376-7388/99/$ – see front matter © 1999 Elsevier Science B.V. All rights reserved.
PII: S0376-7388(99)00143-X

increasing feed concentration. In conventional UF systems, a high recirculation velocity is used to induce hydraulic turbulence which minimizes the accumulation of solute molecules on the membrane surface, thus maintaining an acceptable permeate flux. However, as feed concentration increases, it becomes more difficult to maintain a high recirculation velocity due to an increase in feed viscosity [2,3]. Decoupling the hydraulic cleaning action from recirculation/pressurization can minimize this problem. In the high-shear rotary ultrafiltration (HSRUF) system, disk membranes are rotated at speeds up to 1750 rpm to induce hydraulic turbulence which scours the membrane surface, while the pump is required only to provide transmembrane pressure and a small amount of recirculation flow [4].

A parametric waste-specific study was conducted to provide insight into the relationship between membrane rotational speed, transmembrane pressure, feed MW fluid concentration, and permeate flux, relative to resistance-in-series (RIS) modeling. The applicability of the RIS permeate flux model in representing data collected during the HSRUF treatment of a synthetic oily waste was investigated in a matrix of 18 discrete experiments conducted at constant MW fluid concentration/membrane rotational speed combinations over a range of applied pressures. RIS model parameters (e.g., intrinsic membrane resistance, fouling layer resistance, resistance index, and concentration polarization layer resistance) for the synthetic oily waste stream were determined for each discrete experiment. Based upon observations of the interactions of the resistance index, Φ, with MW fluid concentration and membrane rotational speed, a more specific form of the RIS model was formulated. Additionally, a set-point operating pressure was determined as a function of membrane rotational speed and feed oil concentration such that the resistances R'_m and R_p were minimized.

2. Theory

UF is an alternative treatment option for oily wastewaters, which have traditionally been treated by chemical addition and gravity separation [1]. Reed et al. [5] reported on the treatment of an oily wastewater from the MW industry using tubular UF, resulting in permeate oil/grease (O/G) concentrations of less than 50 mg/l. Lipp et al. [6] presented data on the UF of O/W emulsions with oil and total organic carbon rejections of >99.9% and >96%, respectively. Cheryan [2] summarized the results of several case studies on the use of UF for the treatment of mixed oily wastewaters containing oleic acid and paraffin. Goldsmith et al. [7] reported on the treatment of soluble oil wastes using conventional cross-flow UF in which the waste was concentrated from less than 3% to 40% oil residual with effluent O/G concentrations less than 25 mg/l.

In UF operation, permeate flux is linearly proportional to transmembrane pressure under conditions of low pressure, low solute feed concentration, and high hydraulic turbulence. However, as transmembrane pressure is increased, permeate flux will become independent of transmembrane pressure and will asymptotically approach a limiting value, J^*. The pressure-independent region generally predominates under conditions of high transmembrane pressure, high feed concentration, and low hydraulic turbulence [2,3].

As the permeate passes through the membrane pores, solute particles are convectively transported to the membrane surface and a "concentration polarization" layer is formed. The formation of the concentration polarization layer is the primary reason why the permeate flux for a waste stream is lower than the clean water flux (CWF). The thickness of the concentration polarization layer is reduced by: (1) solute back-diffusion to the bulk solution and (2) tangential fluid flow (i.e., shear force) at the membrane surface [2,3].

In general, membrane fouling (due to solute adsorption onto the membrane surface or membrane pore plugging) occurs under conditions of high feed concentration and low hydraulic turbulence. Lee et al. [8] observed an increased potential for membrane fouling under conditions of high O/W emulsion concentrations and low hydraulic turbulence. The increased fouling potential was attributed to an increase in the probability that oil droplets contacted the membrane surface, were subsequently deformed, and entered the membrane pores. As a result, it is necessary to control operating parameters to minimize the effects of concentration polarization and consequently reduce the potential for membrane fouling [8,9].

2.1. RIS model

In the RIS approach to permeate flux modeling, the layer of particles at the membrane surface is considered to be a physical barrier to permeate flow [2,3]:

$$J = \frac{\Delta P}{R}, \tag{1}$$

where J is the permeate flux (permeate flow rate/membrane area), ΔP the average transmembrane pressure, and R the total resistance to permeate flow. In ultrafiltration, R is composed of three individual resistance terms:

$$R = R_m + R_f + R_p, \tag{2}$$

where R_m is the intrinsic membrane resistance, R_f the fouling resistance, and R_p the concentration polarization layer resistance. R_m is determined using pure water as the feed solution [2]. Typically, R_f is caused by solute adsorption onto the membrane surface and/or membrane pore plugging. Since fouling leads to alterations in the physical makeup of the membrane, R_f and R_m are grouped together to form the total membrane resistance, R'_m:

$$R'_m = R_m + R_f. \tag{3}$$

The concentration polarization layer resistance is related to ΔP by

$$R_p = \Phi \Delta P, \tag{4}$$

where Φ is the resistance index, which is a function of system mass transfer properties (e.g., feed viscosity and hydraulic turbulence.) Combining Eqs. (1)–(4) yields [2,3,10,11]

$$J = \frac{\Delta P}{R'_m + \Phi \Delta P}. \tag{5}$$

Unlike the Hagen–Poiseuille and thin-film models (used to describe the pressure-dependent and pressure-independent permeate flux, respectively), both the pressure-dependent and pressure-independent regions can be predicted using the RIS approach. In the pressure-dependent region the concentration polarization layer is not very thick; thus, $R_p \ll R'_m$ and J is linearly related to ΔP. In the pressure-independent region, the thickness or density of the concentration polarization layer increases and $R_p \gg R'_m$. Under such conditions, J becomes independent of ΔP at a limiting value of $1/\Phi$. In order to increase the pressure-independent permeate flux, it is necessary to reduce Φ by decreasing the feed concentration or increasing hydraulic turbulence [2,3,10,11].

Additionally, it is possible to quantify individual resistances, thus identifying the different flux decline constituents and determining the magnitude of the effect each resistance has on the permeate flux. UF operation can be optimized by determining which resistances are the largest under a given set of operating conditions and taking measures to reduce the magnitude of the resistance term by altering operational parameters [3,9].

Further, Cheryan [2] presented a set-point for UF operation, ΔP_{set}, the pressure at which polarization effects are balanced against the total membrane resistance; thus,

$$\Delta P_{set} = \frac{R'_m}{\Phi}. \tag{6}$$

2.2. HSRUF

A schematic of the HSRUF system is presented in Fig. 1. In the HSRUF system, flat, round membrane disk packs are set on a hollow rotating shaft inside a cylindrical housing. The feed stream enters the membrane chamber under pressure and is distributed across the membrane surface by hydraulic action. The permeate is forced through the membrane under pressure, is collected through the hollow center shaft, and is discharged. The concentrate exits the vessel at the edge of the membrane disk pack. Variations on the mechanically enhanced disk membrane module design have been reported by Kozinski and Lightfoot [12] and Lopez-Leiva [13]. In the HSRUF system, hydraulic turbulence is induced by membrane rotation; thus the pump is only required to provide transmembrane pressure and a small amount of recirculation flow. To further enhance hydraulic turbulence at the membrane surface, stationary turbulence promoters are located on each side of the disk pack. Thus, it is possible to treat highly concentrated wastes using the HSRUF system because the cleaning action is effectively decoupled from feed pressurization/recirculation. Reed et al. [4] reported on the performance of the HSRUF system in which a

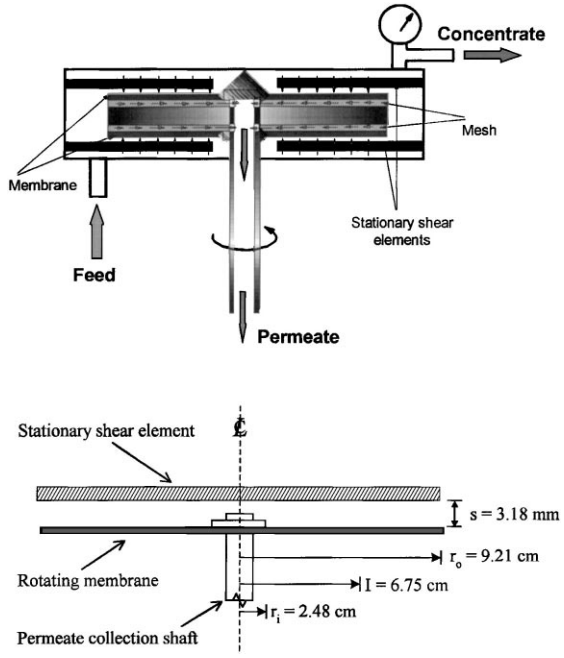

Fig. 1. Schematic of the HSRUF system. Cross-sectional view of membrane vessel (top) and dimensions of the membrane and stationary shear element (bottom).

waste MW fluid was concentrated from an initial concentration of ~5% oil to concentrations as high as 65%.

In the HSRUF system, hydraulic turbulence is achieved by rotating the membrane surface and is characterized by the radial Reynolds Number, Re_r:

$$Re_r = \frac{\omega r^2}{\nu}, \tag{7}$$

where ω is the membrane rotational speed, r the membrane radius, and ν the kinematic viscosity of the feed solution. Ketola and McGrew [14] characterized hydraulic flow conditions as turbulent for $Re_r > 2 \times 10^5$ in a rotary disk membrane system in which the stationary turbulence promoter was a solid plate. However, in this study, the solid plate turbulence promoter was replaced with non-solid "wagon wheel" stationary shear elements. Thus, the transitional Re_r determined by Ketola and McGrew can only be used as an approximate guideline for the cut-off between laminar and turbulent hydraulic flow in the HSRUF system.

In the HSRUF system, permeate is forced toward the outer edge of the membrane by centrifugal force and toward the hollow center permeate collection tube under transmembrane pressure force [15]. Thus, a net decrease in transmembrane pressure is ascertained due to a non-uniformly distributed permeate backpressure, P_b:

$$P_b = \frac{\rho(\omega r)^2}{2}, \tag{8}$$

where ρ is the feed solution density. Thus, the average permeate backpressure, $P_{b(avg)}$, occurs at the radius of gyration of the rotating membrane disk plate:

$$P_{b(avg)} = \frac{\rho(\omega I)^2}{2}, \tag{9}$$

where I is the radius of gyration for a flat rotating ring:

$$I = \sqrt{\frac{r_i^2 + r_o^2}{2}}, \tag{10}$$

where r_i is the inner membrane radius and r_o the outer membrane radius [16]. The average transmembrane pressure, ΔP, is the difference between the applied pressure, P_i, and the average permeate backpressure:

$$\Delta P = P_i - P_{b(avg)}. \tag{11}$$

In the HSRUF system, it is important to maintain operating parameters (P_i and membrane rotational speed) to ensure that the applied pressure is always greater than the maximum permeate backpressure, $P_{b(max)}$ which occurs at r_o. If the applied pressure is less than $P_{b(max)}$, the net driving force and direction of permeate flow will reverse and membrane delamination can result.

3. Experimental

3.1. Experimental apparatus

A schematic of the experimental apparatus is presented in Fig. 2. In the HSRUF system, one 20 cm (8 in) diameter membrane disk pack was set on a hollow rotating shaft inside the vessel housing. The feed stream entered the membrane chamber under pressure and was distributed across the membrane surface by hydraulic action. A constant feed tempera-

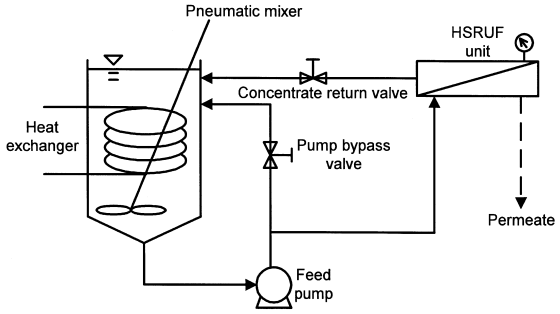

Fig. 2. Schematic of the experimental apparatus.

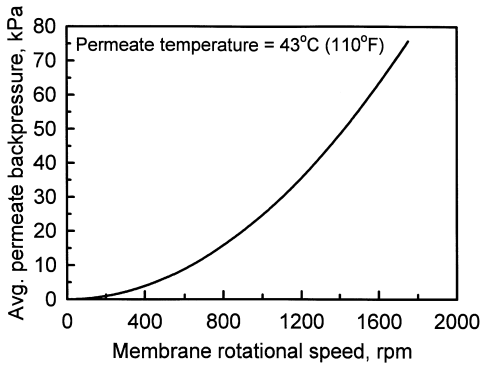

Fig. 3. Average permeate backpressure at typical membrane rotational speeds.

ture was maintained using a heat exchanger located in the feed tank and a pneumatic mixer was used to maintain homogenous feed conditions. To minimize the loss of feed volume due to evaporation of water, a plastic lid with an access port for the pneumatic mixer was kept on the feed tank throughout the duration of each experiment.

3.2. Membrane characteristics

A TRUMEM ceramic membrane (TiO_2/Al_2O_3) with a mean pore size of 0.11 μm and a thickness of 240 μm was used in this study. One of two identical ceramic membranes was mounted on each side of the round disk pack. The physical dimensions of the membrane disk and stationary shear element spacing are presented in Fig. 1, where the inner and outer radii of the membrane were 2.48 cm (0.975 in) and 9.21 cm (3.63 in), respectively, for a total membrane area of 492 cm^2 (0.53 ft^2). The average permeate backpressure over a range of typical membrane rotational speeds (calculated according to Eq. (9)) is presented in Fig. 3.

3.3. MW fluid experiments

A summary of experimental conditions used in each discrete experiment is presented in Table 1. In this study, applied pressure was designated as P_i, membrane rotational speed as R_j, MW fluid concentration as O_k, and oil concentration as OC_k. Experiments were conducted using the HSRUF system in 18 discrete membrane rotational speed/MW fluid concentration combinations. Synthetic feed solutions containing constant MW fluid concentrations ranging from 5% to 40% were freshly prepared from a base MW package in each experiment. The lowest O_k of 5% MW fluid was selected to approximate the initial feed concentration in the treatment of waste MW fluids and the highest O_k of 40% MW fluid was selected to approximate residual concentrations that can be achieved through HSRUF treatment. Membrane rotational speeds of 1150, 1450, and 1750 rpm (the maximum speed attainable on the pilot-scale HSRUF system) were used in this study. P_i ranged from 103

Table 1
Summary of experimental conditions used in each discrete experiment

R_j (rpm)	O_k (% MW fluid)					
	5	10	15	20	30	40
1750	172–517 kPa (25–75 psig)	172–517 kPa (25–75 psig)	138–517 kPa (20–75 psig)	138–483 kPa (20–70 psig)	172–483 kPa (25–70 psig)	172–483 kPa (25–70 psig)
1450	172–517 kPa (25–75 psig)	172–517 kPa (25–75 psig)	172–483 kPa (25–70 psig)	103–483 kPa (15–70 psig)	172–483 kPa (25–70 psig)	138–483 kPa (20–70 psig)
1150	172–517 kPa (25–75 psig)	172–517 kPa (25–75 psig)	103–483 kPa (15–70 psig)	103–483 kPa (15–70 psig)	103–483 kPa (15–70 psig)	103–483 kPa (15–70 psig)

to 517 kPa (15 to 75 psig) to ensure a positive net transmembrane pressure. After each discrete experiment, the membrane was cleaned using a standardized cleaning procedure and a CWF was measured to track the resistance of the membrane over the course of the study.

MW fluid feed solutions were freshly prepared for each experiment in the feed tank by mixing a base MW package in distilled water. The base MW fluid was obtained from a commercial metal manufacturer's rolling mill and contained 85% oil and 15% proprietary additives (e.g., antifoaming agents, film strength additives, etc.):

$$OC_k = 0.85(O_k). \tag{12}$$

Each discrete experiment was conducted under the following experimental conditions: operational mode=recycle (permeate returned to the feed tank); feed volume=40 l (10.6 gal); concentrate return flow rate=3.8+0.8 l min^{-1} (1.0+0.2 gal min^{-1}); and feed temperature=43±1°C (110±2°F). Permeate flux was measured every 5 min for the first 15 min at a given P_i, then every 10–15 min thereafter. P_i was then increased to the next pressure condition and the flux determination procedure was repeated. After the final P_i was reached, the system was shutdown, cleaned, and a CWF was measured. The experimental procedure was then repeated at the next set of discrete R_jO_k conditions.

3.4. Membrane cleaning procedure

The following cleaning procedure was applied initially to the virgin ceramic membrane (to determine the intrinsic membrane resistance), and then after each discrete R_jO_k experiment. After the system was shutdown and drained, the membrane was visually inspected for physical damage. Particular attention was paid to the accumulation/formation of an oily ring or a gel-like layer on the membrane surface as reported by Reed et al. [4]. Following visual observation of the membrane, the system was flushed with hot tap water to displace any residual oil remaining in the unit. After flushing, the system was cleaned for 30 min with a distilled water feed adjusted to a pH of 11.8 with NaOH and 30 ml of an EDTA-containing surfactant (for metal complexation). During cleaning, the system was operated under the following conditions: R_j=1750 rpm; feed temperature=57±1°C (135+2°F) and P_i=276 kPa (40 psig). After base/surfactant cleaning, the system was drained and flushed with hot tap water. The system was then acid cleaned (pH adjusted to 2.2 using H_2SO_4) for 30 min under the same operational conditions used in base/surfactant cleaning and flushed a final time with hot tap water.

After completing the cleaning procedure, a CWF was measured using distilled water under the following operating conditions: R_j=1750 rpm; feed temperature=57±1°C at P_i=172, 345, and 517 kPa (25, 50, and 75 psig, respectively). The system was operated at each P_i condition until the flux stabilized.

3.5. Quality assurance/quality control

$R_{m(water)}$, the resistance of the membrane determined from CWF versus average transmembrane pressure data measured after cleaning, was tracked to determine whether system behavior was biased as a function of time due to changes in membrane characteristics. $R_{m(water)}$ versus experimental identification number (in chronological order) is presented in Fig. 4. An analysis of variance (ANOVA) was conducted to assess the dependence of $R_{m(water)}$ on experimental order. In ANOVA analysis, the F-test statistic was used to determine the contribution of the independent variables in determining the dependent variable. If $F \simeq 1$ it was concluded that there was no association between the dependent and independent variables; if $F \gg 1$, it was concluded that the independent variable contributed to the prediction of the dependent variable

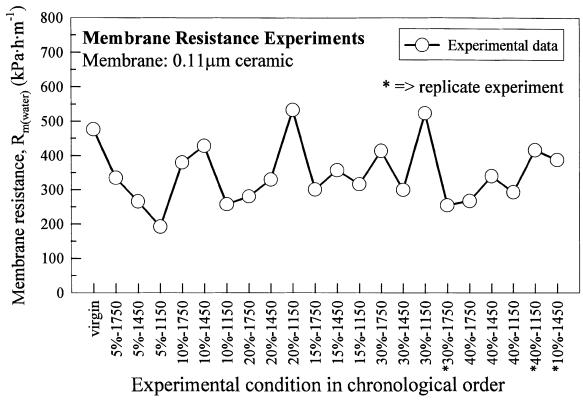

Fig. 4. $R_{m(water)}$ versus experimental identification number (in chronological order).

[17]. Based upon an F-test statistic of 0.4 (calculated at 95% confidence), it was determined that $R_{m(water)}$ did not change significantly; thus, it was concluded that permeate flux data were not significantly biased by changes in membrane characteristics over the course of this study.

4. Results and discussion

Permeate flux at each P_i versus time for the 10%-1750 rpm experiment is presented in Fig. 5. Permeate flux was stable at each P_i and increased in a distinct stepwise pattern as P_i was raised. Average permeate flux versus average transmembrane pressure (calculated using Eq. (11)) for the 10%-1750 rpm, 10%-1150 rpm, and 40%-1750 rpm experiments are presented in Fig. 6. Data presented in Fig. 6 are representative of the broad range of experimental results obtained in this study. In the 10%-1750 rpm experiment (●), flux increased linearly with pressure through 302 kPa (43.8 psi), and then deviated from the linear relationship at higher pressures; however, a constant pressure-independent flux was not established over the pressure range investigated. In the 10%-1150 rpm experiment (■), a linear increase in permeate flux with pressure was evident at pressures less than 277 kPa (40.2 psi). Permeate flux then diverged from the linear pressure–flux relationship at pressures in excess of 277 kPa and a constant pressure-independent permeate flux of 0.38 m h^{-1}

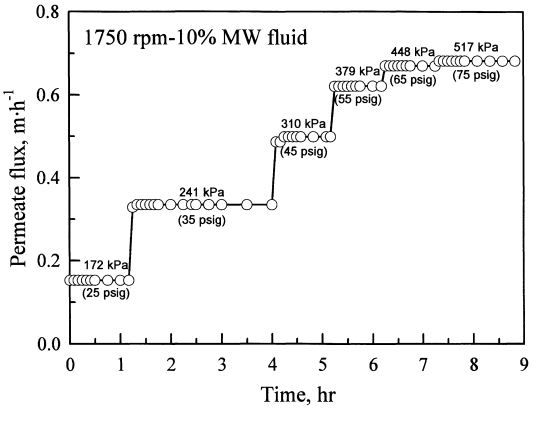

Fig. 5. Permeate flux at each P_i versus time for the 10%-1750 rpm experiment.

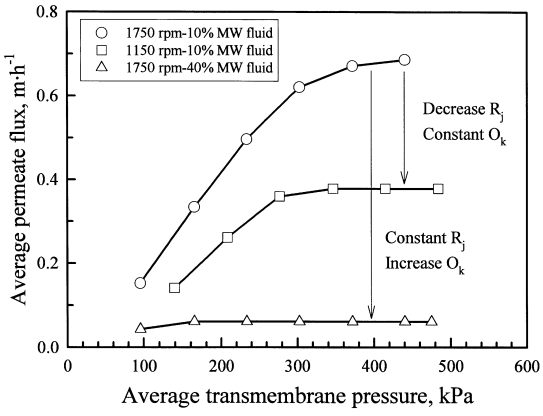

Fig. 6. Average permeate flux versus average transmembrane pressure for the 10%-1750 rpm, 10%-1450 rpm, and 40%-1750 rpm experiments.

(223 gal ft^{-2} d^{-1}) was ascertained. In general, lower permeate flux was observed when R_j was decreased, as observed in the 10% MW fluid experiments conducted at 1750 and 1150 rpm. In the 40%-1750 rpm experiment (▲), a limiting permeate flux of 0.06 m h^{-1} (35.9 gal ft^{-2} d^{-1}) was ascertained at average transmembrane pressures in excess of 165 kPa (9.4 psi). In the data set as a whole, lower permeate flux was observed at each P_i when O_k was increased, as presented in Fig. 6 for the 10% and 40% MW fluid experiments conducted at 1750 rpm. Additionally, the transition from pressure-dependent to pressure-independent permeate flux conditions tended to prevail at lower pressures as R_j was decreased and O_k was increased. Based upon the observations of data similar to those presented in Fig. 6, it was hypothesized that the resistance to hydraulic flow of permeate increased as hydraulic turbulence was decreased and MW fluid concentration was increased.

4.1. Total membrane resistance

To develop the RIS model, pressure–flux data from each discrete R_jO_k experiment were fitted to Eq. (5) using non-linear regression analysis (SigmaPlot® Version 4.0). R'_m values ranged from 123 to 701 kPa h m^{-1} and were comparable to data ranging from 24 to 240 kPa h m^{-1} reported by Nazzal and Wiesner [18] and Lipp et al. [6] for UF membranes used in the treatment of soluble oils.

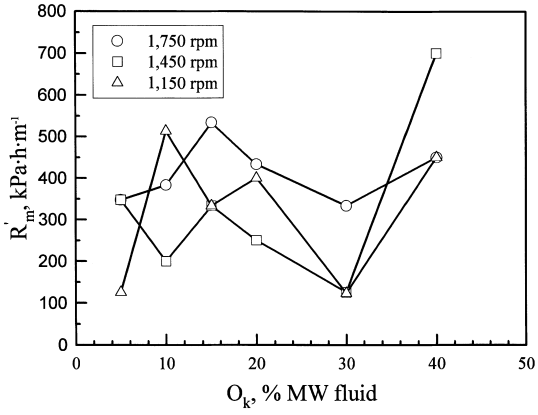

Fig. 7. R'_m versus O_k (at each R_j).

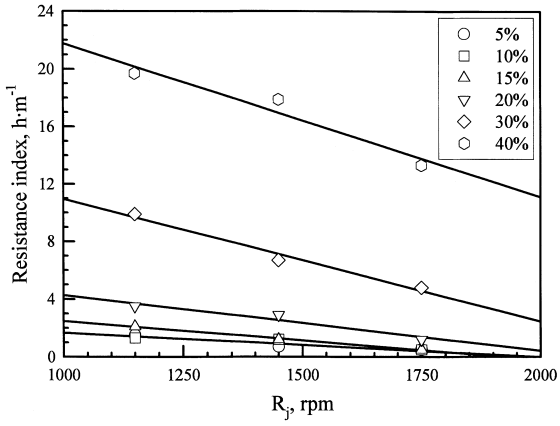

Fig. 8. Resistance index versus R_j (at each O_k).

R'_m versus O_k (at each R_j) is presented in Fig. 7. A two-factor ANOVA was conducted using R_j and O_k as independent variables and R'_m as the dependent variable to assess the prediction of the dependent variable based upon the independent variables. Based on the F-test statistic of 1.1 determined from the data in this study, it was concluded that R'_m was not dependent on either rotational speed or oil concentration. Chiang and Cheryan [10] reported similar results for the UF treatment of skimmilk in a hollow fiber UF system in which R'_m was reported to be independent of hydraulic turbulence (expressed as cross-flow velocity) and feed concentration.

The average R'_m value (of all discrete R_jO_k experiments) was 358 kPa h m^{-1}. The intrinsic resistance of the virgin membrane, R_m, was determined to be 314 kPa h m^{-1} (ascertained using clean water prior to initiating MW fluid experiments). Thus, the average R_f value (based on Eq. (3)) was 43 kPa h m^{-1}, which corresponded to 12% of the average total membrane resistance. As a result of membrane rotation induced hydraulic turbulence, fewer solute droplets accumulated on the membrane surface, effectively minimizing the potential for membrane pore plugging and solute adsorption onto the membrane surface [2,9].

4.2. Resistance index

Values of Φ determined in this study ranged from 0.50 to 19.7 h m^{-1} and were generally lower than those reported for conventional UF separation systems. Chiang and Cheryan [10] reported Φ values ranging from 21 to 120 h m^{-1} in the UF treatment of skimmilk using a hollow fiber UF unit while Wu et al. [11] reported Φ values ranging from 5.0 to 30 h m^{-1} for the treatment of a reactive-dye wastewater in a tubular UF module. However, Φ values for oily wastewaters have not been reported in the literature.

Resistance index versus R_j (at each O_k) is presented in Fig. 8. Φ decreased linearly with R_j over the range O_k examined in this study. Under conditions of high hydraulic turbulence, the thickness of the concentration polarization layer was low, which corresponded to a higher permeate flux as presented earlier in Fig. 6. Resistance index versus O_k (at each R_j) is presented in Fig. 9, as well as MW fluid viscosity versus O_k. For all R_j, the increase in Φ with O_k was similar to the relationship between the absolute viscosity and O_k, as determined in small-scale experiments outside the HSRUF system at 43±1°C. The Φ–O_k and viscosity–O_k relationships can be represented as a second order polynomial [10]. Thus, the resistance index was a function of both membrane rotational speed and MW fluid concentration.

Φ values for the synthetic MW fluid corresponded to polarization resistances ranging from 13.5×10^4 to 1.17×10^4 kPa h m^{-1} over the range of transmembrane pressures examined in this study. When compared with the average total membrane resistance of 358 kPa h m^{-1}, it was determined that the polarization resistance was the predominant rate controlling resis-

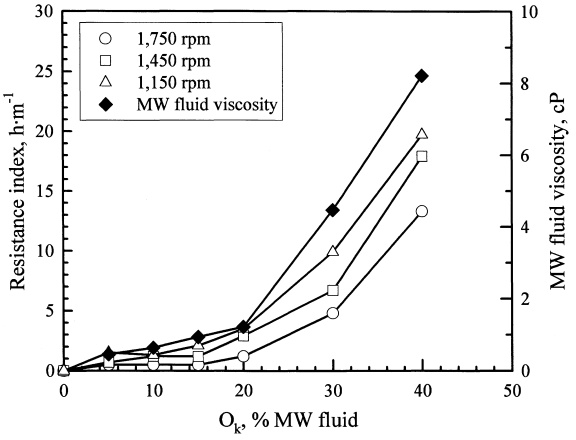

Fig. 9. Resistance index (at each R_j) and MW fluid viscosity versus O_k.

tance in the HSRUF system. Consequently, R_p values were lowest and permeate flux was highest under conditions of low feed concentration (5%, 10%, and 15% MW fluid) and high hydraulic turbulence.

The impact of R_j and O_k on permeate flux is most clearly discerned in the limiting case where the concentration polarization layer is thick or dense (i.e., $R_p \gg R'_m$) and Eq. (5) reduces to

$$J^* = \frac{1}{\Phi}. \tag{13}$$

Limiting permeate flux, J^*, at 1150, 1450, and 1750 rpm versus MW fluid concentration is presented in Fig. 10.[1] At each MW fluid concentration, $J^*_{1750} > J^*_{1450} > J^*_{1150}$; however, the flux advantage obtained by operating at higher membrane rotational speed decreased as the MW fluid concentration was increased to 40%. Average radial Reynolds Number, $Re_{r(\mathrm{avg})}$, at 1150, 1450, and 1750 rpm versus MW fluid concentration is also presented in Fig. 10. A convergence of $Re_{r(\mathrm{avg})}$ values, similar to the J^*–O_k relationship, was observed as the MW fluid concentration was increased. Consequently, the decreased flux advantage was primarily attributed to the increased influence of

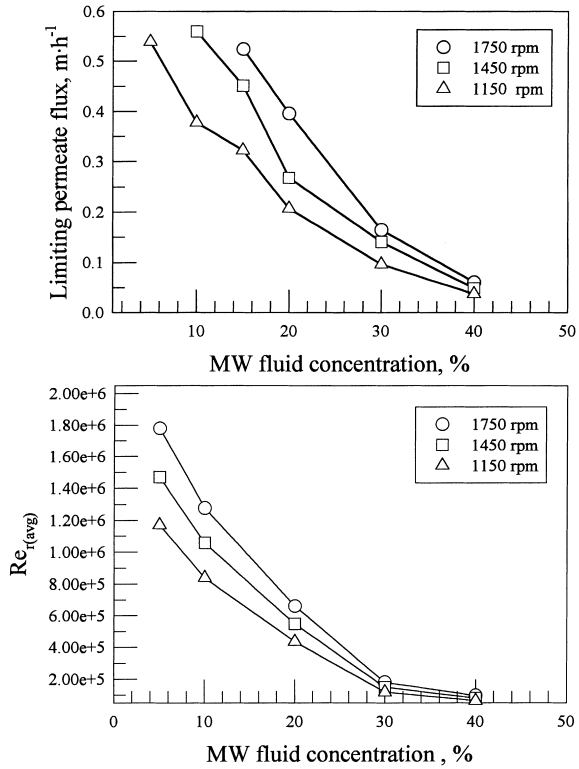

Fig. 10. Limiting permeate flux at 1150, 1450, and 1750 rpm versus MW fluid concentration (top) and average radial Reynolds number at 1150, 1450, and 1750 rpm versus MW fluid concentration (bottom).

viscosity on hydraulic turbulence and a corresponding increase in the resistance to hydraulic flow of permeate at higher MW fluid concentrations.

A power-law relationship is often used to gauge the effect(s) of hydraulic turbulence on the limiting flux, where [2]

$$J^* = f(Re)^n. \tag{14}$$

Cheryan [2] summarized typical n values for conventional tubular UF systems of 0.3–0.6 when operated under laminar flow conditions and 0.8–1.2 for turbulent flow. However, Viadero and Reed [15] reported an exponent value ranging from 1.4 to 1.5 (determined in experiments conducted using the same synthetic MW fluid presented in this investigation), further suggesting a strong relationship between membrane rotational speed and permeate flux in the HSRUF system.

[1] A limiting permeate flux was not observed for the 5% and 10% MW fluid experiments conducted at 1750 rpm, though a deviation from pressure-dependent to pressure-independent behavior was observed, as presented previously in Fig. 6 for the 10%-1750 rpm experiment.

4.3. Modification of the RIS model

Since Φ was a function of both R_j and O_k as presented in Figs. 8 and 9, a more specific form of the resistance index was postulated:

$$\Phi = \underbrace{a_0 + a_1 R_j}_{\substack{\text{linear} \\ \Phi, R_j \\ \text{relationship}}} + \underbrace{a_2\, OC_k + a_3 (OC_k)^2}_{\substack{\text{polynomial} \\ \Phi, O_k \\ \text{relationship}}}, \tag{15}$$

where a_0, a_1, a_2, and a_3 are curve fitting parameters. In full-scale UF operations, waste MW fluids are typically characterized by their oil content; thus, OC_k values were used in the postulated form of Φ. The first two terms of Eq. (15) represent the linear relationship between Φ and R_j as observed in Fig. 8. The third and fourth terms represent the second order polynomial relationship between Φ and O_k (and therefore OC_k) as observed in Fig. 9. Thus, the modified form of the RIS model was

$$J = \frac{\Delta P}{R'_{\mathrm{m}} + \left[a_0 + a_1 R_j + a_2\, OC_k + a_3 (OC_k)^2\right] \Delta P}, \tag{16}$$

where a_0=3.40, a_1=-8.44×10^{-4}, a_2=-0.11, and a_3=1.32×10^{-2}. Modified RIS model results and experimental data for representative $R_j OC_k$ combinations are presented in Fig. 11. The hypothetical relationship between J, ΔP, R'_{m}, R_j, and OC_k presented in Eq. (16) adequately predicted both pressure-dependent and pressure-independent permeate flux behavior. The modified form of the RIS model presented in Eq. (16) was not intended for a priori flux prediction; rather, the relationship was used as an approach toward developing a more complete understanding of the effect(s) of operating parameters on permeate flux in the rotary disk UF separation system. Given the magnitude of the R_j and OC_k terms in Eq. (16), feed oil concentration was the predominant parameter contributing to an elevated polarization resistance and consequently a lower permeate flux as observed in the case of the limiting flux data presented in Fig. 10.

HSRUF systems in the field will likely be run at a constant, elevated, membrane rotational speed to minimize the potential for membrane fouling [4]; thus, further efforts to minimize R'_{m} and R_{p} were focused on optimizing the relationship between ΔP and OC_k. Based upon Eq. (6) and the form of Φ presented in Eq. (15), the set-point transmembrane pressure in the HSRUF system was given as

$$\Delta P_{\mathrm{set}} = \frac{R'_{\mathrm{m}}}{a_0 + a_1 R_j + a_2\, OC_k + a_3 (OC_k)^2}. \tag{17}$$

ΔP_{set} at 1150, 1450, and 1750 rpm versus oil concentration is presented in Fig. 12. In the HSRUF system, it is possible to operate at a constant membrane rotational speed while adjusting the transmembrane pressure to maintain ΔP_{set} as a waste is concentrated because pressure and hydraulic turbu-

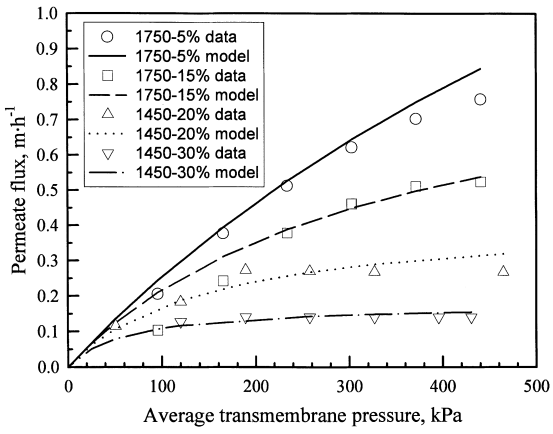

Fig. 11. Modified RIS model results and experimental data for representative $R_j OC_k$ combinations.

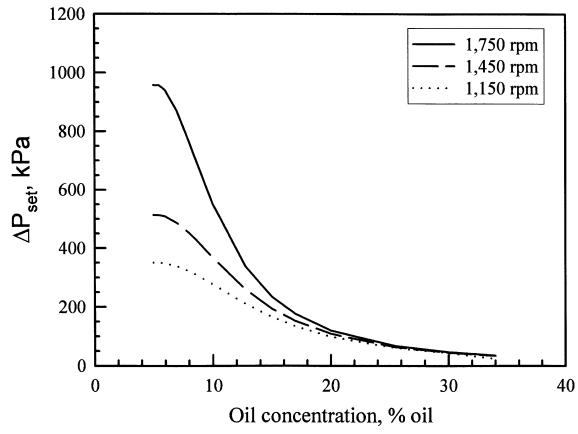

Fig. 12. ΔP_{set} at 1750, 1450, and 1150 rpm versus oil concentration.

lence can be varied independently; unlike conventional UF separation systems in which pressure and cross-flow velocity are generally coupled.

Based upon the convergence of ΔP_{set} at elevated feed concentrations for each of the three rotational speeds presented in Fig. 12, an additional operating strategy is to decrease both membrane rotational speed in addition to transmembrane pressure as the feed concentration is increased. Thus, operating costs associated with both pumping and rotation can be minimized, while balancing polarization and fouling effects in the HSRUF system. However, Reed et al. [4] reported significant membrane fouling and a loss of permeate flux when membrane rotational speed was first decreased then increased in the HSRUF treatment of a waste MW fluid. The turbulence excursions reported by Reed et al. were conducted during the course of a direct concentration experiment. Consequently, effects due to aging of the feed solution and feed deterioration under high temperature and shear force may have also adversely affected membrane performance. However, Fane and Fell [9] also reported similar results in which a negligible increase in permeate flux was attained when hydraulic turbulence was increased in a tubular UF module. Thus, operation at elevated membrane rotational speeds may be necessary from a practical perspective when treating waste MW fluids in direct concentration runs to minimize the increased potential for membrane fouling at high feed concentrations.

5. Conclusions

The relationship between permeate flux, transmembrane pressure, membrane rotational speed, and feed concentration in the high-shear rotary ultrafiltration (HSRUF) of a synthetic metal working (MW) fluid was ascertained and the application of the RIS model was evaluated. A series of 18 discrete experiments were conducted at constant membrane rotational speed/MW fluid concentration combinations over a range of transmembrane pressures to determine the relationship between RIS model parameters, feed solution characteristics, and system operating conditions. Based upon experimental observations, the RIS model was modified and a working relationship between permeate flux, membrane rotational speed, and feed oil concentration was established. The modified RIS model was not intended for a priori flux prediction; however, the revised form of the model was used to develop a better understanding of the interaction between operating parameters and permeate flux in the HSRUF system. Additionally, a setpoint operating pressure was determined as a function of oil concentration such that the resistances R'_m and R_p were minimized. The following specific conclusions are forwarded:

(1) Membrane resistance after cleaning, $R_{m(water)}$, did not change significantly over the course of this study; thus, the membrane cleaning procedure was effective at restoring membrane performance after each discrete experiment and the data were not biased by changes in membrane characteristics.

(2) Total membrane resistance and resistance of the fouling layer, R'_m and R_f, respectively, were not influenced by membrane rotational speed or feed MW fluid concentration. Additionally, R_f was determined to be only 12% of R'_m; thus, the potential for membrane pore plugging and/or solute adsorption onto the membrane surface is effectively minimized through the efficient transfer of "cleaning energy" to the membrane surface via membrane rotation.

(3) Polarization resistance, R_p, is the predominant rate controlling resistance in the treatment of synthetic MW fluids in the HSRUF system. The deleterious effects of increased polarization resistance can be minimized through membrane rotation induced hydraulic turbulence, since polarization resistance decreases with increased membrane rotational speed. However, the effects of rotation induced hydraulic turbulence decrease as MW fluid concentration is increased due to an increase in MW fluid viscosity. As pilot-scale HSRUF systems are scaled up, the high permeate flux and low fouling and polarization resistances obtained by operating at high membrane rotational speeds must be weighed against the corresponding increase in operating costs as a feed stream is concentrated.

(4) The modified RIS model, based upon the interactions of the resistance index with membrane rotational speed and feed MW fluid concentration, adequately predicts permeate flux data from discrete experiments. Thus, the modified model may be used to predict permeate flux at intermediate $P_iR_jO_k$ conditions in the experimental matrix, though flux predic-

tion outside the range of experimental conditions examined in this study must be based upon an extrapolation of data.

(5) Fouling and polarization resistances can be minimized by maintaining the optimum transmembrane pressure, ΔP_{set}, as the MW fluids are concentrated. By operating at or near ΔP_{set}, enhanced operating efficiency, operational cost savings, and an extension of the membrane life cycle can be achieved.

(6) The experimental approach and conclusions regarding the interaction of permeate flux with membrane rotation and feed MW fluid concentration serve as: (1) a basis to broaden the scientific evaluation of the HSRUF system by establishing a benchmark for future comparisons; and (2) a step toward understanding the interaction between permeate flux, membrane rotational speed, and feed concentration, thus enhancing the application and operating efficiency of systems in the field.

6. Nomenclature

I	radius of gyration for a flat rotating ring (cm)
J	permeate flux (m h^{-1})
J^*	pressure-independent permeate flux (m h^{-1})
OC_k	oil concentration (% oil)
O_k	MW fluid concentration (% MW fluid)
P_b	permeate backpressure (kPa)
$P_{b(avg)}$	average permeate backpressure (kPa)
$P_{b(max)}$	maximum permeate backpressure (kPa)
P_i	applied pressure (kPa)
R	total resistance to permeate flow (kPa h m^{-1})
R_f	fouling resistance (kPa h m^{-1})
R_j	membrane rotational speed (rpm)
R_m	intrinsic membrane resistance (kPa h m^{-1})
$R_{m(water)}$	clean water resistance determined after cleaning (kPa h m^{-1})
R'_m	total membrane resistance (kPa h m^{-1})
R_p	concentration polarization layer resistance (kPa h m^{-1})
r	membrane radius (cm)
r_i	inner membrane radius (cm)
r_o	outer membrane radius (cm)
r_p	membrane pore radius (cm)
Re_r	radial Reynolds Number (dimensionless)
$Re_{r(avg)}$	average radial Reynolds Number (dimensionless)
ΔP	average transmembrane pressure (kPa)
ΔP_{set}	set-point operating transmembrane pressure (kPa)
ρ	feed solution density (kg l^{-1})
ν	kinematic viscosity of the feed solution (cSt)
ω	membrane rotational speed (rpm)
Φ	resistance index (h m^{-1})

References

[1] J. Burke, Waste treatment of metalworking fluids. A comparison of three common methods, Lubric. Eng., April (1991) 238.

[2] M. Cheryan, Ultrafiltration and Microfiltration Handbook, Technomic Publishing, Lancaster, PA, 1997.

[3] A. Jonsson, G. Tragardh, Fundamental principles of ultrafiltration, Chem. Eng. Process. 27 (1990) 67.

[4] B. Reed, W. Lin, R. Viadero, J. Young, Treatment of concentrated oily wastes using centrifugal membrane separation (CMS), J. Environ. Eng. 123(12) (1997) 1234.

[5] B. Reed, W. Lin, C. Dunn, P. Carriere, G. Roark, Treatment of an oil/grease wastewater using ultrafiltration: pilot-scale results, Sep. Sci. Technol. 32(9) (1997) 1493.

[6] P. Lipp, C. Lee, A. Fane, C. Fell, A fundamental study of the ultrafiltration of oil–water emulsions, J. Membr. Sci. 36 (1988) 161.

[7] R. Goldsmith, D. Roberts, D. Burre, Ultrafiltration of soluble oil wastes, J. Wat. Pollut. Control Fed. 46(9) (1974) 2183.

[8] S. Lee, Y. Aurelle, H. Roques, Concentration polarization, membrane fouling, and cleaning in ultrafiltration of soluble oil, J. Membr. Sci. 19 (1984) 23.

[9] A. Fane, C. Fell, A review of fouling and fouling control in ultrafiltration, J. Membr. Sci. 62 (1987) 117.

[10] B. Chiang, M. Cheryan, Ultrafiltration of skimmilk in hollow fibers, J. Food Sci. 51(2) (1986) 340.

[11] J. Wu, M. Eiteman, S. Law, Evaluation of membrane filtration and ozonation processes for treatment of reactive-dye wastewater, J. Environ. Eng. 124(3) (1998) 272.

[12] A. Kozinski, E. Lightfoot, Protein ultrafiltration: A general example of boundary layer filtration, AIChE J. 18(5) (1970) 1030.

[13] M. Lopez-Leiva, Ultrafiltration at low degrees of concentration polarization: technical possibilities, Desal. 36 (1980) 115.

[14] H. Ketola, J. McGrew, Pressure, frictional resistance, and flow characteristics of the partially wetted rotating disk, J. Lubric. Technol., April (1968) 395.

[15] R. Viadero, B. Reed, in: J. Boardman (Ed.), Effects of Membrane Rotation on the Performance of the Centrifugal Ultrafiltration Separation System, Proc. 29th Mid-Atlantic Industrial and Hazardous Waste Conference, Roanoke, Virginia, 13–16 July 1997, Technomic, Lancaster, PA, 1997, p. 614.

[16] A. Arya, Classical Mechanics, Allyn and Bacon, Needham Heights, MA, 1993.

[17] A. Bowker, G. Lieberman, Engineering Statistics, 2nd ed., Prentice-Hall, Englewood Cliffs, NJ, 1972.

[18] F. Nazzal, M. Wiesner, Microfiltration of oil-in-water emulsions, Water Environ. Res. 68(7) (1996) 1187.